

AERODYNAMIC PERFORMANCE INCREASE OF AN A320 MORPHING WING IN SUBSONIC REGIME

Xavier Delon [1, 2], Jacques Abou Khalil [2,3,4], Nils Maynard [2, 4], Abderahman Marouf [1], Rajaa el Akoury [2], Yannick Hoarau [1], Carsten Doll [3], Jean-François Rouchon [4] and Marianna Braza [2]

[1] ICUBE Laboratoire des sciences de l'Ingénieur, de l'Informatique et de l'Imagerie, UMR 7357 CNRS-Univ. Strasbourg ENGEES-INSA, 4 Rue Blaise Pascal, 67081, Strasbourg, France

:

[2] IMFT Institut de Mécanique des Fluides de Toulouse, Unité Mixte C.N.R.S.-I.N.P.T. 5502, All. du Prof. Camille Soula, 31400 Toulouse, France

[3] ONERA, DTIS, Toulouse, France, 31400.

[4] LAPLACE Laboratoire Plasma et Conversion d'Energie, UMR 5213 CNRS-INPT-UT32 Rue Charles Camichel, 31071 Toulouse, France

xdelon@unistra.fr , xavier.delon@imft.fr

Abstract

This study investigates the effect of a novel electroactive morphing concept based on a "live-skin", composed of a significant number of piezo-actuators able to deform and vibrate with optimal frequencies, amplitudes and wavelengths. This "skin" forms a streamwise travelling wave (TW) actuation and is disposed along strategic areas of the lifting structure's suction side to considerably increase the aerodynamic performance. This new morphing approach has been experimentally implemented on the "Large Scale" (LS) high-lift A320 morphing prototype of the HORIZON-2023-2027-PATHFINDER Project N° 101129952-BEALIVE-"Bioinspired Electroactive multiscale Aeronautical Live skin", http://horizon-europe-bealive.eu/ .

The experiments have been conducted in the S1 wind tunnel of the IMFT regarding the take-off flight phase in low subsonic regime at 2° of incidence, Reynolds number of 2.25 million and a Mach number of 0.037 is studied. The total chord of the LS prototype in "clean" is of 2.40 m and of 2.70 m in take-off. Three rows composed of 28 piezo-actuators each are disposed near the area of 89% of the total chord and towards of the trailing edge of the high-lift flap suction side. Local sinusoidal deformations of the flap surface have been created at vibration frequencies in the range (4, 256) Hz with a wavelength of 9 cm and vibration amplitude in the order of 1 mm at a fixed voltage of 700 V. The comparisons between the static (non-actuated) configuration and the actuated ones reveal a significant increase of the lift force (+7.91%) and a drag reduction of −0.47% with the "live-skin". The averaged flow dynamics have also been investigated numerically by using the Navier-Stokes Multi Block (NSMB) code [1]. The simulations provided the modification of the near wake structure thanks to the morphing, as well as the impact on the main turbulence quantities, turbulence stresses and kinetic energy.

1. Introduction

Due to the significant increase in aviation fuel consumption, which aggravates air pollution and accelerates global warming, the scientific community must face important challenges to overcome this expansion. A key factor is to reduce the fuel consumption needed by the commercial aviation, which represents almost 90% of the whole aviation industry [2], by improving the aerodynamic performances and thus reducing the emission of gases such as, CO_2 and NO_X. Indeed, these objectives are aligned with the European long-term strategy for sustainable aviation. The Flightpath 2050 vision published by ACARE and the European Commission sets targets of a 75% reduction in CO_2 emissions per passenger-kilometre, a 90% reduction in NO_X emissions and a 65% reduction in perceived noise relative to year-2000 aircraft (Flightpath 2050).

The wing design received a great impetus for all the flight phases since the onset of aviation up to nowadays by means of wind tunnel experiments and since the '90's up to now through with CFD numerical simulations, performed more recently on supercomputers. Significant advances have been obtained over the last thirty years thanks to these approaches. To enhance the gain in performances, a bio-inspiration of different animals such as, owls, birds of prey, sharks, stingray among other, provides novel morphing concepts able to "mimic' fundamental mechanisms obtained by these animals.

Thanks to shape modification as well as of the vibratory character of specific parts of the wings, the understanding and optimisation of the fluid-structure-interaction has been obtained, able to adapt to changing environmental conditions.
In the context of the strong inter-disciplinary research synergy among the Institutes IMFT, LAPLACE and ICUBE, a number of studies were conducted during the last fifteen years towards novel morphing concepts for the future wing design, partly bio-inspired, [3,4]. The partial only bio-inspiration is due to the fact that the afore mentioned animals are not faced to the real velocity and time scales of an aircraft's flight. These studies produced disruptive wing prototypes equipped of different classes of electroactive materials, able to operate at a multitude of time and length scales, as required by the turbulence spectrum nature. Therefore, the *hybrid electroactive* morphing was derived for the first time in the literature [5,6,7], simultaneously associating Shape Memory Alloys (SMA) for high deformations at low frequency (order of 1Hz), similar to the cambering of large span hunting birds to increase lift and specific piezoceramic actuators able to vibrate in higher frequencies (order of hundreds of Hz) with slight deformations, as the feathers of birds or the scales of sharks. The electrical actuation ensured a light morphing (comparing to MEMS and hydromechanical actuators), able to act instantaneously and to need small energy consumption (in the order of 50 W for one linear m of span), thus ensuring an economic concept. The fluid-structure interaction physical mechanisms engendered by this kind of morphing were thoroughly investigated through refined experiments [6] and simulations [8].
In the context of other studies, the European research projects SARISTU and AFLONEXT, as well as studies in the framework of CleanSky (https://www.clean-aviation.eu/clean-sky-2), included coordinated research initiatives regarding morphing wings capable of dynamic camber adjustments and trailing-edge modifications [9] and [10].
The H2020 N° 723402 European project "SMS" - "Smart Morphing and Sensing for aeronautical configurations", www.smartwing.org/SMS/EU and
https://cordis.europa.eu/project/id/723402) [11] coordinated by the Institut de Mécanique des Fluides de Toulouse (IMFT) reported a significant increase of the lift-to-drag ratio of 8% on a near full-scale (1:1) Airbus-320 wing prototype, achieved through camber modification of the high-lift flap using SMA for the landing configuration [11]. Furthermore, a 1.3% lift-to-drag increase was obtained by Hi-Fi numerical simulations in take-off configuration around a complete Airbus-320 equipped with the hybrid morphing (optimal cambering shape with trailing edge vibrations). Indeed, imposing optimal monochromatic trailing edge vibrations along the span using piezoceramic actuators of Micro-Fiber Composite (MFC) type allowed suppression of three-dimensional instabilities arising in low subsonic regime corresponding to take-off conditions, [8] and [12]. In the transonic regime corresponding to cruise conditions, a significant drag reduction in the order of 9% and a lift-to-drag improvement of 6 % was achieved through a row piezoactuators along the trailing edge, [13] combined with a slight upwards deformation of the trailing edge area. In fact, these actuators were able to manipulate the near-wake turbulence by producing small coherent vortex structures that interact with the existing coherent structures in the shear layers and in the near wake thereby creating vortex breakdown drastically modifying the upstream wall pressure distribution. Thanks to this feedback effect, these actuations were able to attenuate the buffet instability, [14].
The overall research carried out in the SMS project demonstrated that a slight modification of the shape coupled with optimal frequency vibrations with an amplitude of around 1 mm in the near the trailing edge area and vibration frequencies between 100 Hz and 300 Hz, have a noticeable impact on the main flow instabilities even upstream of the actuated zone. The shear layer instability forming Kelvin-Helmholtz vortices are thus weakened when hybrid morphing is implemented. This leads to the "sweep" of the von-Kármán vortex shedding much farther downstream in the wake. These effects simultaneously produce an increase in lift, a decrease in drag and reduce noise sources. A time-dependent vibration frequency (wobulation) has been also investigated [11] and proven able to instantaneously detect optimal frequency ranges to apply as a monochromatic actuation leading to aerodynamic performance increase, [15].
Furthermore, a numerical study was carried out by [16] in which the hybrid morphing (cambering + flapping effects) was implemented on the near full-scale Airbus 320 wing prototype and also on the whole aircraft. The simulations were launched at two different Reynolds numbers: 2.25 and 7 million for different angles of attack in take-off and different high-lift flap cambered positions with an actuated frequency of around 300 *Hz* allowing 1 mm of trailing edge amplitude. For the 3D simulations of the whole aircraft, the modelled Reynolds number was fixed at 11 million for the same incidences analysed in 2D simulations with only one specific camber of the high-lift flap corresponding to the optimal one with the same actuation frequency of the trailing edge. Indeed, the hybrid morphing allowed simultaneously an increase in lift-to-drag ratio and decrease in frequency peaks in turbulence spectrum associated with aero noise sources.

The present study has been conducted in the framework of the European project HORIZON-2023-2027-PATHFINDER-Open Project N° 101129952-BEALIVE-"Bioinspired Electroactive multiscale Aeronautical Live skin", http://horizon-europe-bealive.eu/ aiming to develop a morphing actuation system based on the materialisation of streamwise Travelling Waves (TW) forming a "live-skin" in strategic regions of the lifting surface of a wing, with the objective of improving aerodynamic performance.
The "live-skin" morphing concept aims at increasing even more the aerodynamic performance by means of a high degree of freedom of actuation elements composing the "live-skin". Four key parameters are considered regarding the TW

actuation: the wavelength (λ), the vibration frequency (f), the amplitude (a) and the zone of interest on the suction side ($x_0/c, x_f/c$). In this work, the morphing effects are considered on the near full-scale Airbus-320 wing prototype called Large-Scale (LS) at Reynolds number of 2.25 million, an angle of incidence at 2° and 8°. The "live-skin" actuation is implemented exclusively on the suction side of the high-lift flap. Static and morphing configurations have been analysed by means of a detailed experimental campaign in the S1 wind tunnel of the IMFT in synergy with numerical simulations.

The article is organized as follows: section 2 provides the experimental parameters, and how the "live-skin" morphing concept is implemented on the high-lift flap. Section 3 details the numerical method with the turbulence modelling used. Section 4 details the numerical parameters to model the "live-skin" actuation through Travelling Waves. Section 5 provides discussion on the results. The flow dynamics of the static cases (baseline configuration) are first discussed for two incidences of 2° and 8°. The effects of the morphing are analysed in the third and fourth parts of section 5. The aerodynamic performances are evaluated and analysed through unsteady pressure signal postprocessing. In the last section, the effects of the "live-skin" morphing concept on the LS configuration are investigated by means of detailed time-averaged flow dynamics indicating the modification of the surrounding turbulence due to morphing. This is linked to the obtained aerodynamic performances.

2. Experimental approach

As previously mentioned, experiments were carried out in the S1 wind tunnel of the IMFT. This facility is an Eiffel-type open-circuit wind tunnel. The open test section diameter is about 2.4 m and 2 m long. The entry section includes a honeycomb structure designed to regulate the airflow and reduce the natural turbulence intensity, which is around 0.1 %. The upstream velocity in the open test section is ranging from 1 to 35 m/s.

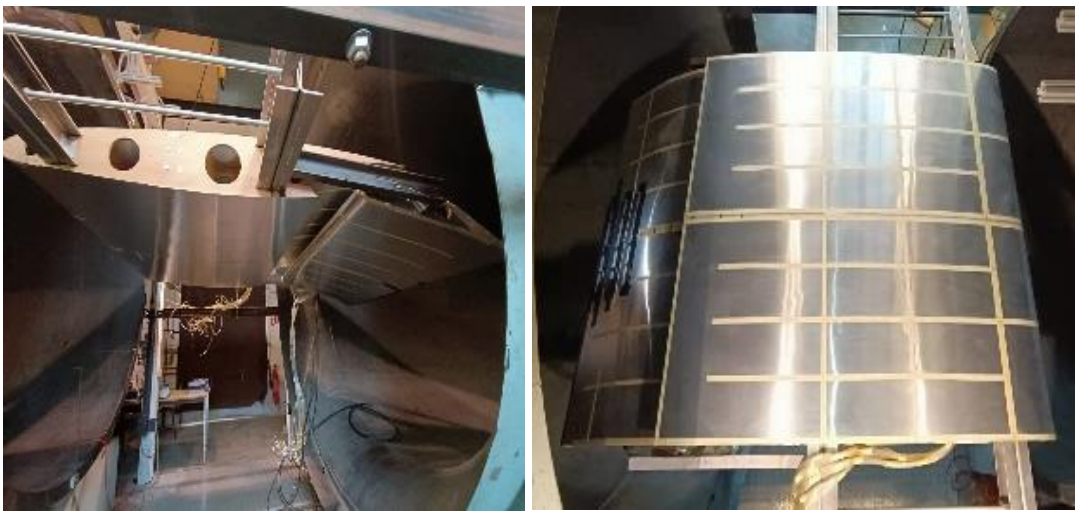


Figure 1. Large-Scale (LS) A320 prototype composed of a fixed-part and of a high-lift flap having a total chord in take-off of 2.70 m and a span of 2m in the S1 wind tunnel of IMFT.

The A320 LS wing prototype consists of two elements as illustrated in Fig. 1. It is composed of a fixed-part of 1.4 m long and the high-lift flap with a chord of 1.0 m yielding a total take-off chord of 2.70 m. The spanwise dimension is of 2 m. In the analysed take-off configuration, the flap is deflected at $\delta = 10°$.

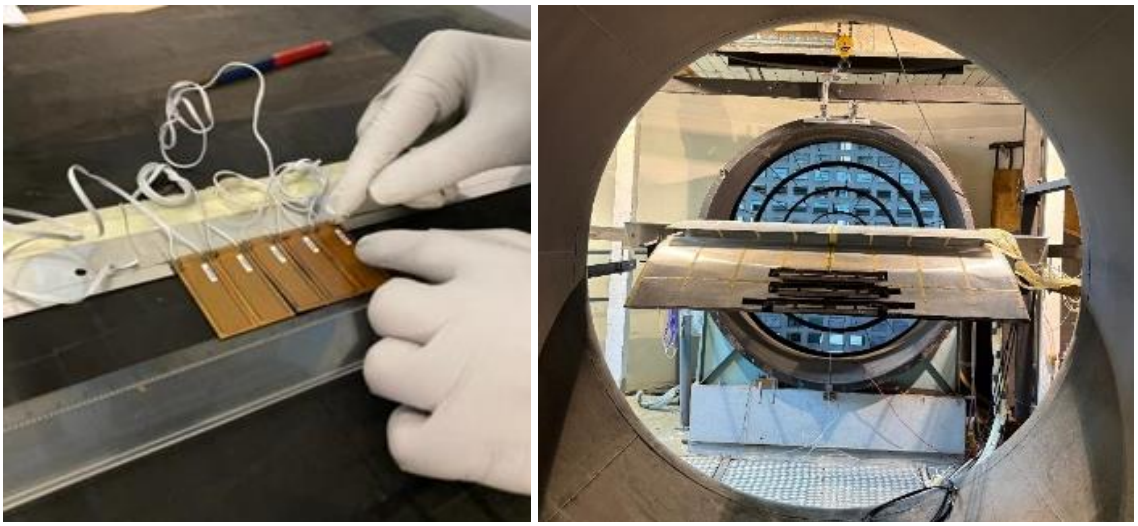


Figure 2. Implementation of the piezoactuators, (left) for one row of the "live-skin" having a length of 58 cm and composed of 28 actuators. The live-skin morphing system is implemented on the flap with three rows (right).

The "live-skin" morphing consists of three rows of piezoceramic actuators implemented near the 89 % of the total A380 wing chord, up to the trailing edge of the flap. A single piezoactuator is 5.3 cm long and 1.8 cm wide. They are mounted on a 58 cm thin metallic bar, which is then fixed to the flap. These rows are spaced 9 cm apart from each other, see Fig. 2. The vibration amplitude is in the order of 1 mm, based on previous studies of the present research group, where it was reported that actuating with higher amplitudes than 2 mm is harmful for the performances because of considerable perturbation of the flow, leading to drag increase [17].

In the present study, the first experimental campaign was carried out at a Reynolds number of 2.25 million corresponding to an upstream velocity of 12.5 m/s. To enable accurate determination of the pressure coefficient C_p along the whole configuration, a dense array of LMI ("Low Measurement Indicator") pressure sensors was applied on the middle spanwise section of the LS prototype. These sensors are defined by their high sensitivity to ultra-low-pressure range, down to 25 Pa as positive or negative increment, making them suitable for aerodynamic measurements. Moreover, a MEGGITT unsteady pressure transducer has been located at 77 % of the flap's chord with a sampling frequency of 6000 Hz. This transducer is coupled with an analog filter unit designed to suppress high-frequency electrical noise and eliminate interferences produced within wind tunnel environment.

3. Numerical method and turbulence modelling

Two-dimensional numerical simulations have been carried out using the Navier-Stokes Multi-Block (NSMB) code [1], with a conservative finite volume method. The governing equations are the time-dependent compressible Navier-Stokes equations. An artificial compressibility numerical scheme [18] allowed accurate computations in the present low Mach number regime. The numerical domain is subdivided into 65 blocks composed of quadrilateral cells. The computation is therefore parallelized across the different blocks according to the procedure implemented in NSMB. For the time discretization, a second order backward differencing is used as implicit temporal scheme. A dual time-stepping [19] is employed to obtain an optimal convergence through an inner iteration algorithm within the outer time step. A fourth-order central skew-numerical scheme coupled with a fourth-order artificial dissipation [20] were used for the convective and a second-order central scheme for the diffusion terms diffusive terms of the N-S equations.

Regarding the turbulence modelling, the Organized Eddy Simulation (OES) approach, [21], [22] and [23] to physically capture the coherent structures development. This approach is based on the ensemble-averaging decomposition of the physical variables in respect of the turbulence spectrum splitting in one part (the resolved part) regrouping the coherent effects and a second part (to be modelled), regrouping the chaotic effects.

The simulated domain and the computational mesh of 734,050 elements leading to an y^+ value $\ll 1$, have been chosen based on previous convergence studies carried out in the SMS European project. In addition, the present mesh has been refined near the actuated zone. The mesh deformation has been considered through the Arbitrary Lagrangian Eulerian (ALE) approach, [24]. The numerical domain (Fig. 3) is willingly larger than the experimental one to quantify more

accurately the flow around the LS configuration in a non-confined environment corresponding to the real flight conditions. The numerical time step is $dt = 10^{-5} s$, according to previous studies in the SMS and BEALIVE European projects.

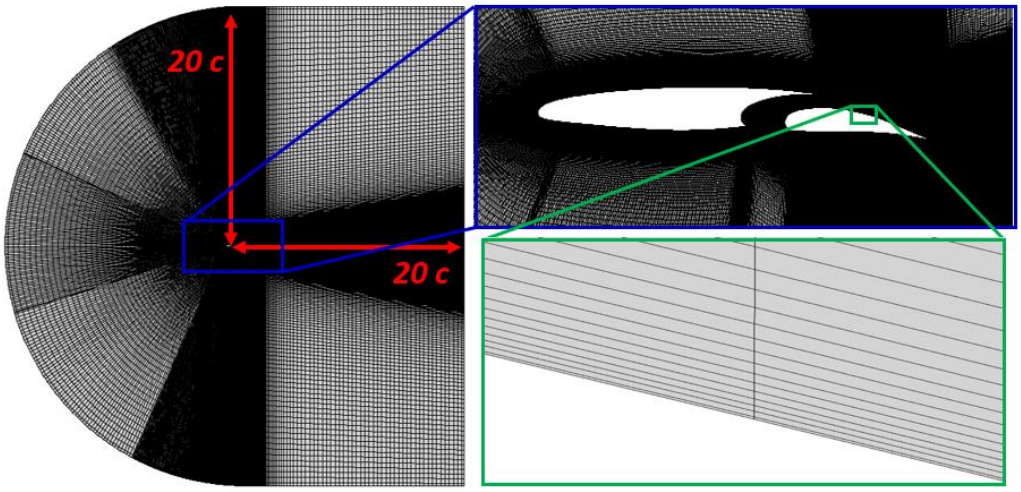


Figure 3. Mesh around the high-lift wing configuration in 2D configuration.

All the simulations were initialized with steady freestream conditions at a constant incoming velocity of 12.5 m/s. Given a reference pressure (101325 Pa) and temperature (293.15 K), this corresponds to a Reynolds number of 2.25 million and a Mach number of 0.036. The turbulent intensity in the incoming flow in the S1 wind tunnel is in the order of 0.1%.

4. Numerical morphing parameters

The "live-skin" morphing has been modelled as a deformation of the suction side surface according to a Travelling Wave (TW) whose parameters are the same as for the "live-skin" actuation. This deformation (Fig. 4), is imposed on the mesh with the Arbitrary Lagrangian-Eulerian (ALE) methodology, [24]. The TW is defined as a sinusoidal deformation with specific smoothing at the beginning and at the end of the implementation zone as detailed in Eq. 1:

$$y(x,t) = \begin{cases} \frac{x-x_0}{x_1-x_0}\, a \sin(kx - \omega t + \Phi) & \text{if} \quad x \in [x_0, x_1] \\ a \sin(kx - \omega t + \Phi) & \text{if} \quad x \in [x_1, x_2] \\ \frac{x_f-x}{x_f-x_2}\, a \sin(kx - \omega t + \Phi) & \text{if} \quad x \in [x_2, x_f] \end{cases} \quad (1)$$

where x_0 and x_f refer to the starting and final coordinates of the wave formation on the high-lift flap's suction side. To avoid divergence on the calculations induced by significant mesh deformations, a smoothing effect is applied on the modelled TW. The factor $\frac{x-x_0}{x_1-x_0}$ smoothly increases from 0 ($x = x_0$) to 1 ($x = x_1$), while the factor $\frac{x_f-x}{x_f-x_2}$ decreases from 1 ($x = x_2$) to 0 ($x = x_f$). Between x_1 and x_2 the overall amplitude of the TW remains constant (Fig. 4).

In Eq. 1, k represents the wavenumber ($k = 2\pi/\lambda$) in $rad.cm^{-1}$, a defines the imposed amplitude of the TW in mm and ω refers to wave angular velocity ($\omega = 2\pi/f$) in $rad.s^{-1}$.

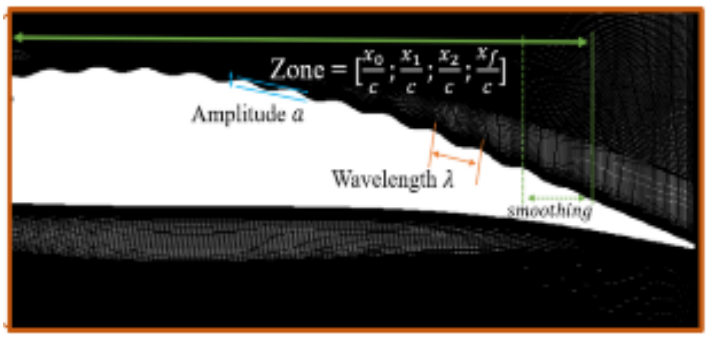


Figure 4. Schematic representation of the Travelling Wave (TW) modeling implemented on the suction side of the high-lift flap according to eq. (1).

5. Results

5.1. Flow structure and dynamic

The LS configuration is composed of two elements, the fixed wing and the high-lift flap. In-between a gap area is formed that affects the flow around the flap. This last can be considered as an aerodynamic profile subjected to the effects of the fixed wing on the flow structure upstream of the flap's leading edge with its own stagnation point. There is a strong interaction between the fixed part and the high-lift flap. The flow structure around the LS configuration is very complex, as illustrated in Figures 5 and 6. In the gap area, Fig. 5 shows coherent small Kelvin-Helmholtz vortices that rap around the leading edge of the flap and form a shear layer along the suction side of the flap. The interaction of the two parts and of the gap structure leads to four shear layers shown in Fig. 6 characterised by streamwise undulations due to the development of shear layer instability. This effect is more intense in case of a higher incidence (Fig. 6) because of the increased shearing rate.

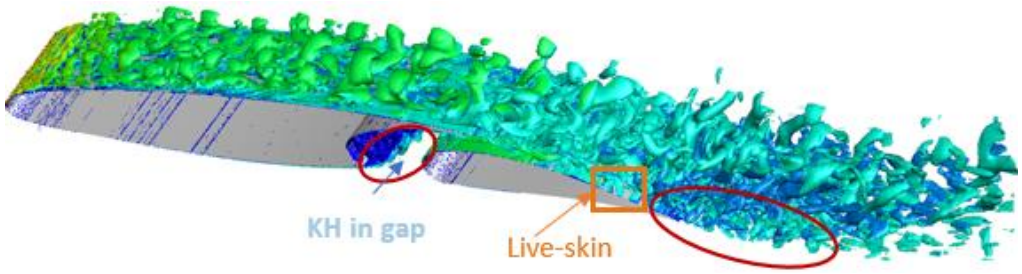


Figure 5. Q-criterion iso-contours coloured by the velocity magnitude illustrating the turbulent flow structure around the A320 - LS prototype at fixed wing incidence of 8° by means of Delayed Detached Eddy Simulation with embedded Organised Eddy Simulation, DDES-OES, [16].

In Fig. 5, spanwise velocity perturbations cause the primary instability vortices to develop spanwise waviness as result of amplification of secondary instability. This secondary instability enhances the streamwise vorticity within the shear layers, ultimately leading to the formation of hairpin vortices

The shear layer instability leads to Kelvin-Helmholtz (KH) vortices that interact farther downstream and form a von Kármán vortex street regarding the two upper shear layers and a lower vortex street concerning the interaction of the two lower shear layers (Fig. 6 a). In Fig. 6 b), the undulation exists but it is less visible due to the low incidence of 2°.

(a)

(b)

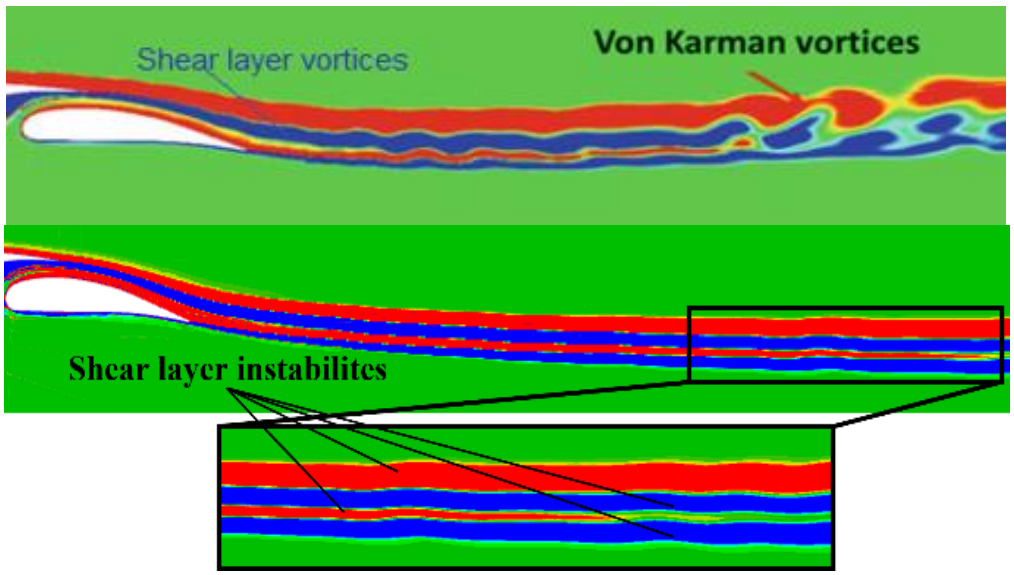


Figure 6. Iso-vorticity contours around the LS prototype: **(a)** static (non-actuated) configuration at incidence of 8°, [16] and **(b)** same configuration at incidence of 2°.

The "live-skin" morphing aims at enhancing the interactions between the solid structure's actuated zone and the fluid, thus affecting the different shear layers and their interfaces among them. Under optimal morphing parameters, the induced interactions can produce coherent vortex breakdowns resulting in shear layer thinning and reduction of the wake's width, thus producing drag reduction with simultaneous reinforcement of the coherent vortices turning in the same direction as those created by the morphing. This can result on enhancement of the vorticity in the upper and lower shear layers where the size of the vortices has been constricted. The enhancement of the vorticity contributes to lift increase along the same mechanisms as in [8]. These modifications, thanks to naturally existing feedback effects due to practically instantaneous propagation of the downstream perturbations in the upstream area, can *produce significant modification of the wall pressure distribution up to the leading edge of the fixed wing* as will be shown experimentally in a next section.

5.2. Static (non-actuated) case

In this section, both experimental and numerical results of the baseline configuration (static, non-actuated) at 2° of incidence are investigated.

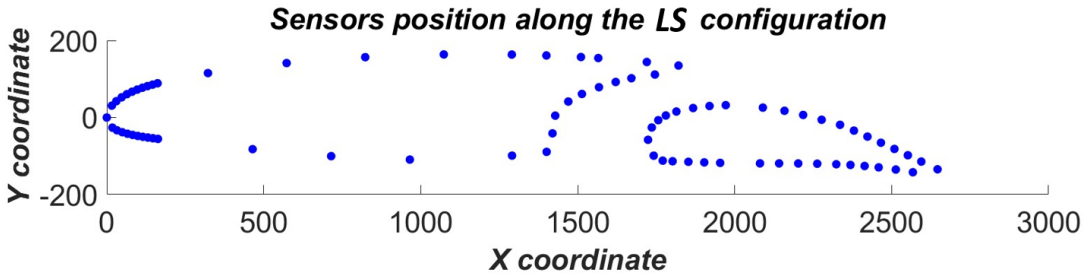


Figure 7. Position of the pressure sensor tabs along the mid-span of the LS configuration.

On the Large-Scale experimental prototype, eighty LMI ("Low Measurement Indicator") static pressure sensors are located along the whole configuration as illustrated in Fig. 7, allowing a detailed mean wall pressure distribution investigation at mid-span and an accurate characterization of the pressure contribution on the lift and drag forces. The mean wall pressure coefficient C_p, at mid-span of the LS configuration is described in Fig. 8 for the static (unactuated) configuration.

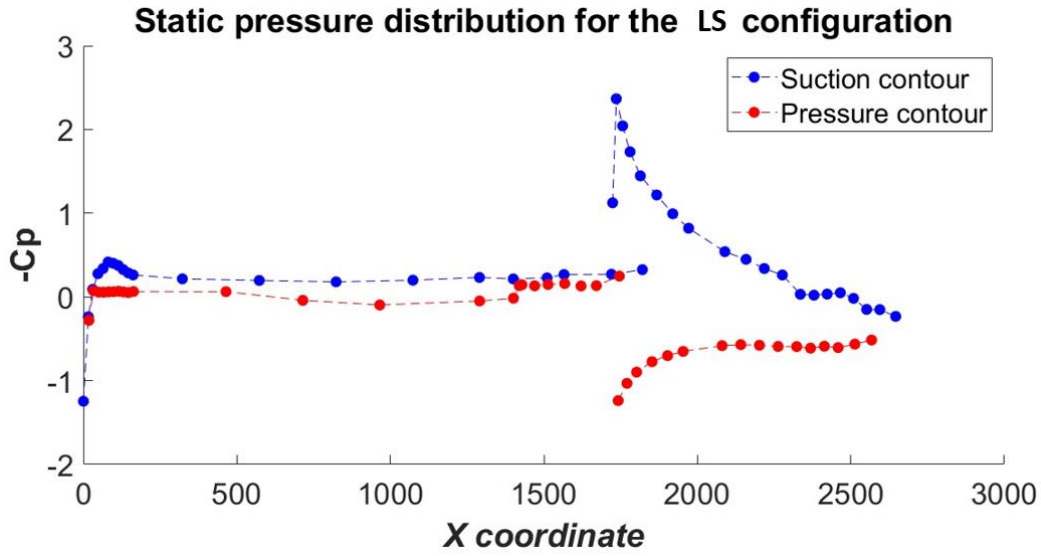
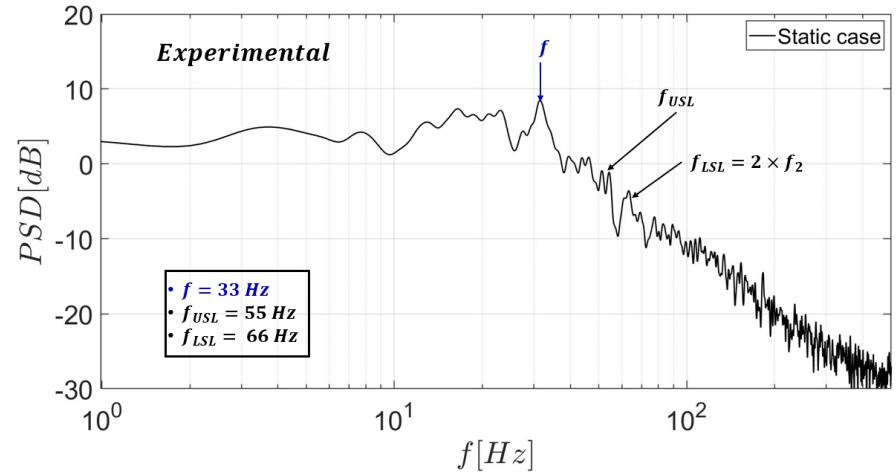


Figure 8. Mean wall pressure coefficient distribution along the LS configuration, static (unactuated) case.

The pressure contribution on the aerodynamic forces of lift and drag has been calculated by integrating the vertical and horizontal elementary forces in respect of the pressure lift and drag contributions.

The unsteady pressure measurements have been carried out at the position $(x/c, y/c) = (0.77, 0.030)$ on the suction side of the flap. A detailed analysis of the recorded signals was made with different approaches, specific to signal postprocessing, (Fig. 9).

(a)



(b)

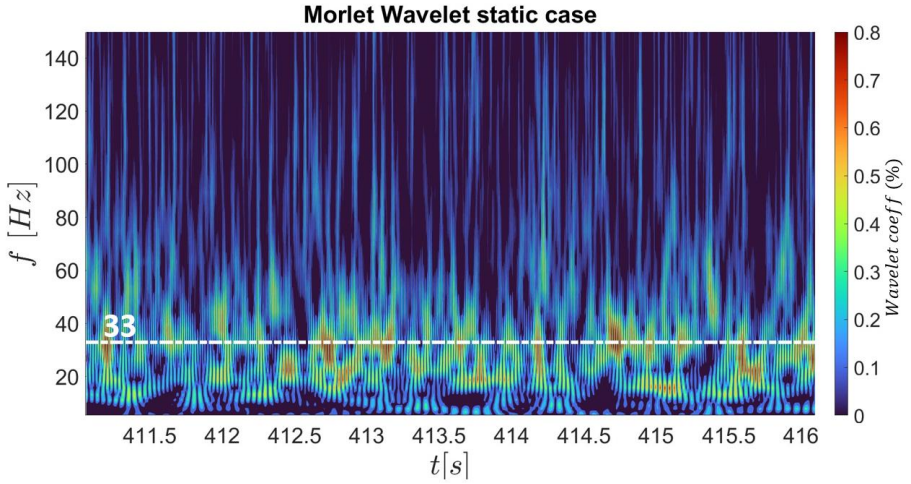


Figure 9. Signal post-processing of the experimental static unsteady pressure signal: **(a)** Power Spectral Density (PSD), **(b)** Morlet's continuous Wavelet transform.

The predominant frequencies are illustrated in Fig 9a corresponding to the most representative coherent structures developed from amplification of the shear layer instabilities. Similar characteristic frequencies are highlighted at the same location as the MEGGITT transducer, see Fig. 10.

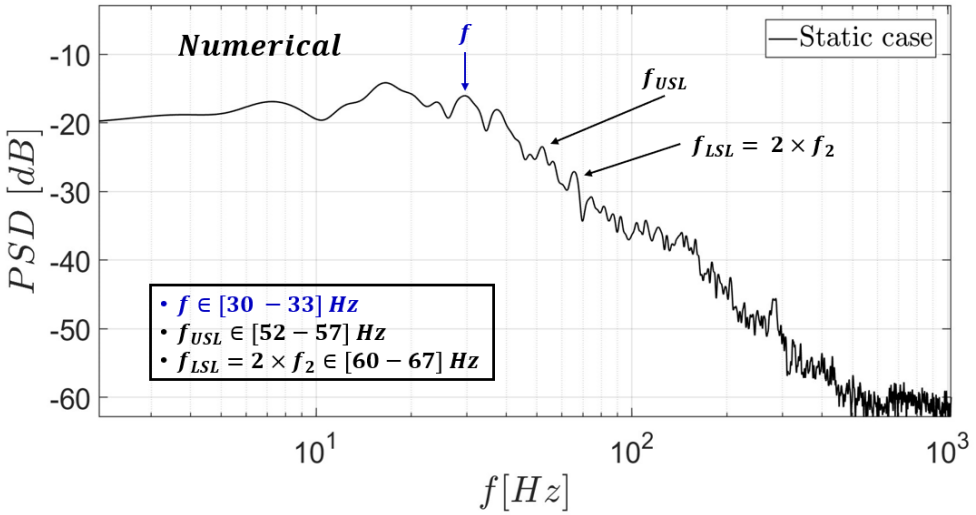


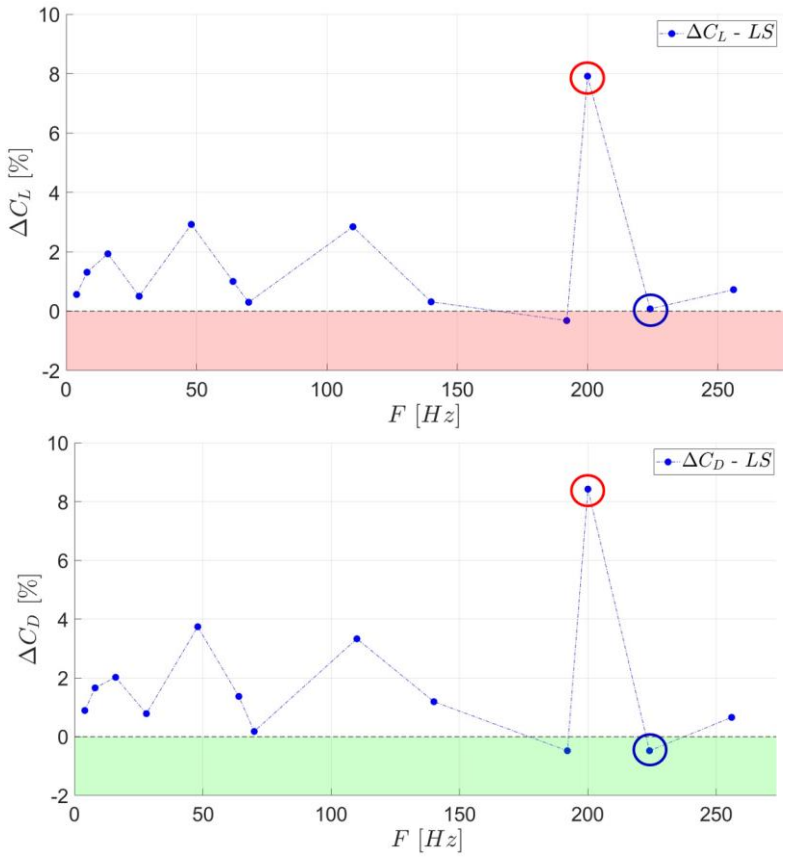
Figure 10. Power Spectral Density (PSD) on the unsteady pressure signal recorded at the numerical monitor point located at $(x/c, y/c) = (0.77, 0.030)$ at the suction side of the flap.

The frequency f is associated with the von Kármán vortex streets illustrated in Fig. 6. The Morlet wavetransform (fig. 9 shows predominance of this frequency and of its harmonic. The spectra indicate also the upper and lower shear layer frequencies.

5.3. Travelling wave morphing cases

The experimental parameters for the "live-skin" modelling have been chosen considering the length scales of the piezoceramic actuators and the distance between the live-skin rows. The actuated region has been located in analogy to former and current studies carried out on the fixed wing "Intermediate-Scale"- (IS) prototype of the BEALIVE project having a chord of 0.7 m, [25]. In this case, separation starts at 70% of the chord. For this reason, as a first exploration, the "live-skin" has been implemented on the LS near the same position in respect of the high-lift flap's chord which is close to t the one of the IS prototype, (details are provided in a companion paper at the same Conference by J. Abou-Khalil) and given that the incidence is similar for the two experimental campaigns.
The actuation frequencies applied on the LS prototype by means of three rows of actuators have been chosen in the range of (50, 250) Hz according to these studies on the IS prototype.

The experimental performances in lift, drag and lift-to-drag ratio have been calculated by considering the pressure contribution on the forces as previously mentioned. Figure 11 presents the modifications due to the morphing versus the actuation frequencies. Two interesting configurations stand out in this experimental campaign. First, the 200 Hz ($\approx 9 \times f_1$) case provided a significant increase in lift ($+7.91\%$) . The drag coefficient increases ($+8.42\%$). This case may be interesting in landing phase with a crucial need in lift increase where drag increase is also needed to reduce the aircraft's speed. In the present case the aerodynamic performance modification has slightly decreased to -0.47%. Second, the case of 224 Hz ($\approx 7 \times f$) produces a slight increase in lift ($+0.0764\%$) with simultaneous drag reduction (-0.48%). The resulting aerodynamic performance is increased to ($+0.56\%$), Fig. 11 with blue circles. This second configuration highlights a good compromise in take-off conditions and illustrates *the ability of the present morphing to produce drag reduction simultaneously to lift increase, although the overall shape has been cambered* due to the high-lift flap. This particular case can be linked to experiments carried out in the frame of the SMS European project [11] where a simultaneous increase of lift and decrease in drag were also obtained with an optimal cambering of the flap and hybrid morphing with trailing-edge small deformation applied on the LS prototype in landing phase.



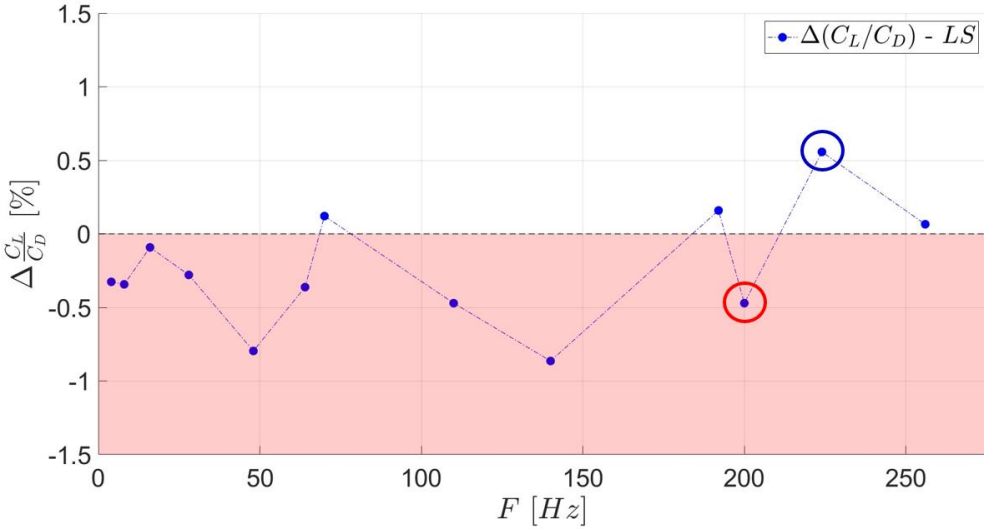


Figure 11. Experimental modification (in percentage) of the pressure lift and pressure drag calculated between the non-actuated and the corresponding morphing case $[\Delta(\%) = 100 \times (\overline{X_{Morph}} - \overline{X_{Stat}})/\overline{X_{Stat}})]$. Top: lift coefficient, middle: drag coefficient and bottom: ratio lift-to-drag coefficient.

The averaged wall pressure coefficient C_p highlights the significant impact of the morphing actuation on the whole prototype for the 200 Hz vibration frequency, Fig. 12.

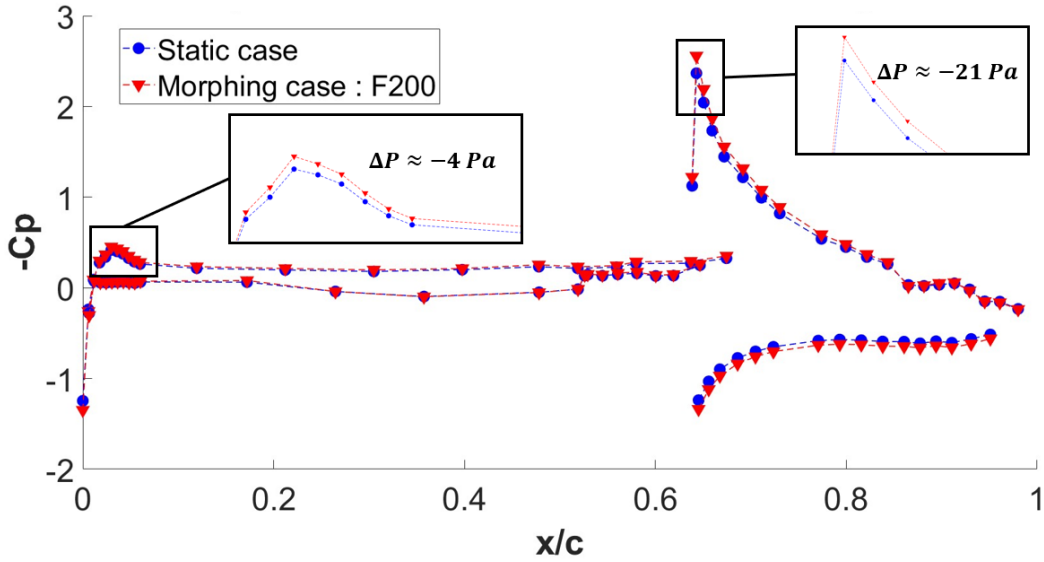


Figure 12. Mean wall pressure coefficient distribution along the LS prototype. Comparison between the static case and the morphing at 200 Hz.

On the suction side the static pressure becomes more negative. This phenomenon is noticed on the whole LS configuration, ***up to the leading edge of the fixed wing*** resulting in lift increase. Moreover, the pressure increases along the intrados too, producing a further lift increase. The highest Δp arises in the flap area but it propagates up to the leading edge of the fixed wing thanks to the afore mentioned naturally existing feedback effects. *These aspects reinforce the strategy of acting through the morphing on the rear wing part to obtain significant benefits up to the most upstream area*. In the case of 224 Hz actuation, the order of magnitude of the performances is considerably lower than the ones obtained at 200 Hz . Nevertheless, the simultaneous increase in lift and notable decrease in drag is an advantage of the present morphing for the take-off flight phase as previously mentioned.

The PSD, as well as the time-dependent frequency modulation, drastically change for these two actuated configurations. The actuation frequency injects a certain amount of energy into the flow illustrated in Fig. 13a) and 13b). The injected

energy amplifies the characteristic frequencies previously analysed. Significant strengthening of the shear layer and von Kármán modes are produced for the 224 Hz configuration while 200 Hz empowered the upper shear layer frequency.

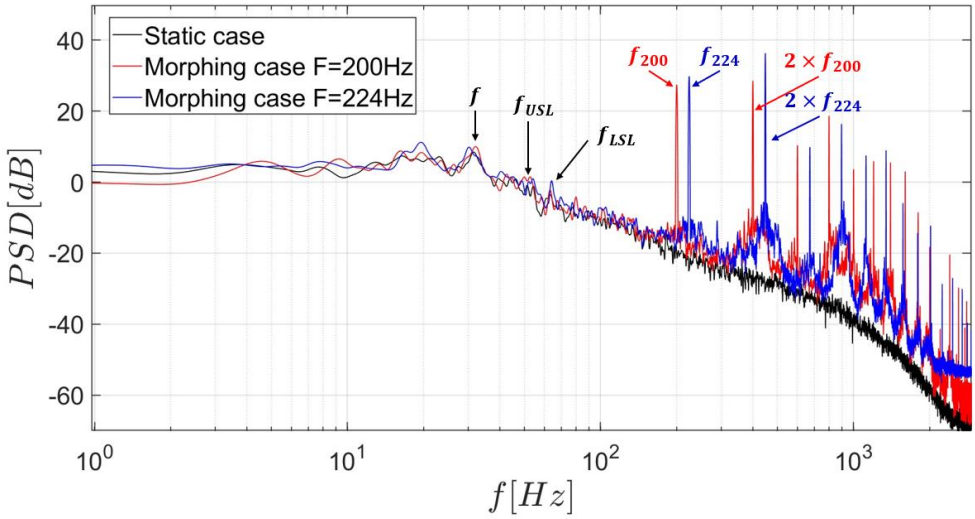


Figure 13a. Power Spectral Density (PSD) of the pressure fluctuations for the three experimental cases: static case, 200 Hz and 224 Hz actuations - experimental results.

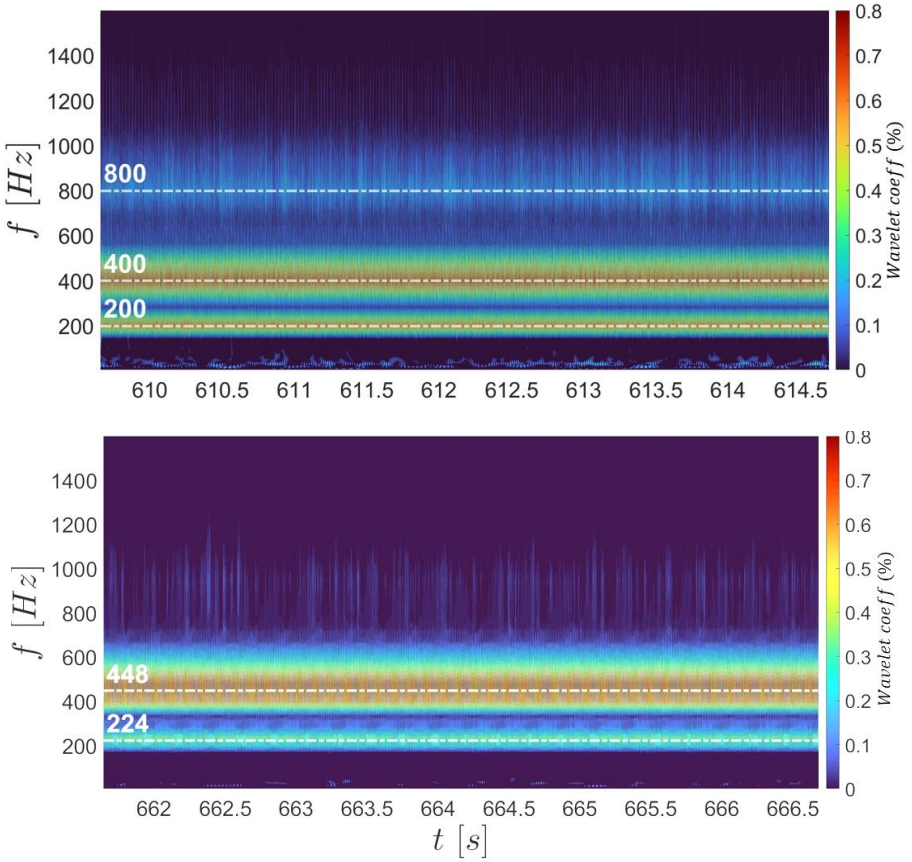


Figure 13b. Morlet's continuous wavelet transform on the unsteady pressure fluctuations for 200 Hz (top) and 224 Hz (bottom). Experimental results.

In addition, the whole frequency content of the recorded signals is organized differently, see Fig. 13.
For the 200 Hz case, the first and second harmonics of the actuation frequency are predominant. This is due to the peaks in the PSD, represented in Fig 12, having the same order of magnitude.

For the 224 Hz configuration, the first harmonic of the actuation frequency is the most representative of the frequency modulation of the recorded signal. The peak is therefore more important than the fundamental one. This pattern causes a contraction of the overall frequency content at around 448 Hz resulting in a more regular signal.

5.4. Numerical investigation of the flow structure

A detailed analysis of the average wake structures was carried out numerically in order to explain the natural modifications induced by the "live-skin" morphing.

For the two actuated configurations the average field of the turbulence production term P_{12} is plotted in Fig. 14. This term is also considered as the work of deformation of the mean flow by the turbulent stresses, defined in Eq. 2 :

$$P_{12} = -\overline{uv} \times \frac{\partial \bar{U}}{\partial y} \tag{2}$$

The superposition with the vertical dimensionless profiles of $P_{12}^{*} = P_{12} \times (c/U_{\infty}^{3})$ was added to better understand the impact of the actuation on the flow. The coloured curves represent the morphing configuration while the dark ones refer to the static case. Each bump forming the profile defines a specific shear layer in the wake. Significant reductions of P_{12} are highlighted by the visualisation of these profiles, especially just downstream of the flap. This aspect is caused by the "live-skin" morphing for which smaller coherent structures are generated locally by the TW actuation into the shear layers. These induced coherent structures perturbate the interactions between the mean motion and the already exiting turbulent flow. Therefore, less energy is extracted from the mean motion through work of deformation by the P_{12} turbulent stresses.
Furthermore, the amplitude of the bumps changes comparing the two actuated configurations. At 224 Hz the first (at the top) and last (at the bottom) bumps remain slightly higher than the one of the 200 Hz. This phenomenon can be linked to the amplification of specific patterns already highlighted in Figures 9a and 12.

6. Conclusion

The experiments carried out at the S1 wind tunnel of the IMFT have highlighted considerable impacts of the new "live-skin" morphing concept on the aerodynamic performances. The Large-Scale (LS) prototype of 2.7 m chord has been studied in take-off configuration. Three rows of piezoceramic actuators were implemented at 89% of the total chord on the high-lift flap. The study was conducted in a low subsonic regime ($M \approx 0.036$) at $Re = 2.25 \times 10^{6}$ and 2° angle of attack. Numerical simulations using the same parameters as in experiments have been simultaneously performed to better understand the impact of the morphing, modelled though a streamwise surface traveling wave (TW) actuation, on the flow dynamics and on the turbulence production into the wake.

The evaluation of the measured aerodynamic forces based on the pressure distribution has identified two interesting configurations for this first experimental campaign. The 200 Hz actuation yielded to a significant increase of $+7.91\%$ in lift coupled with a drag increase $+8.42\%$. This increase is viewed as beneficial for the landing phase where the aircraft's speed has to be reduced. The 224 Hz configuration provides an interesting effect of simultaneous lift increase of $+0.0764\%$ coupled with a drag reduction of -0.478%. The resulting aerodynamic performance has been increased by $+0.557\%$.

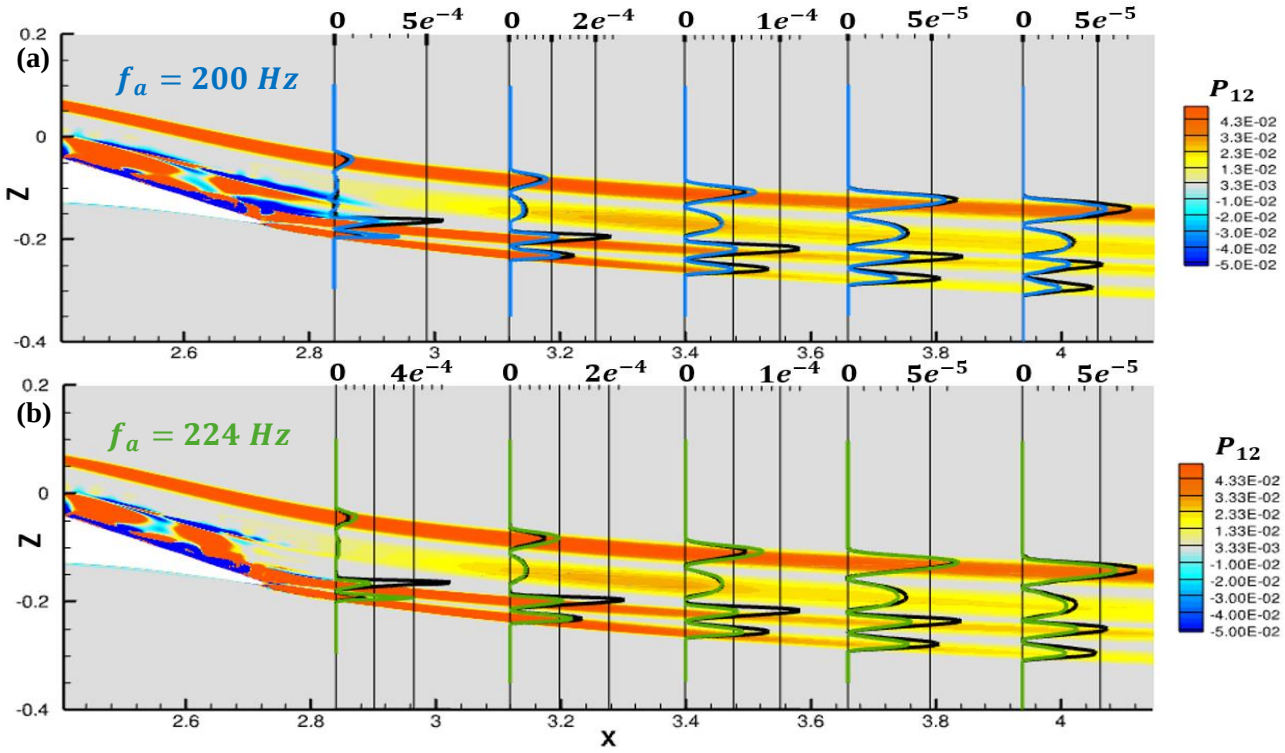


Figure 14. Iso-contours of the turbulence production term P_{12} for: **(a)** 200 Hz and **(b)** 224 Hz actuations. Vertical profiles of dimensionless P_{12} are superimposed showing comparison with the corresponding static case in black colour.

This actuated configuration is particularly interesting in the take-off configuration. The wall pressure modification due to the live-skin morphing has been registered up to the leading edge of the LS prototype due to the naturally occurring feedback effects of the fluctuations arising in the downstream region that are instantaneously propagating up t the most remote upstream area in the present low subsonic regime.
The effect of the "live-skin" morphing on the flow has been analysed with spectral analysis and wavelet transforms in the experiments as well as in the simulations. The "live-skin" morphing induces a significant decrease of the turbulence production term.

This paper has proven that the "live-skin" morphing is able to improve the aerodynamic performance on a near full-scale Airbus-320 high-lift wing/flap prototype. The results presented the potential of the "live-skin" morphing concept towards energy saving and greening of air-transport.

Acknowledgements

The authors are grateful to the Engineering and Technical services of IMFT laboratory enabling the installation of the LS prototype with the accurate implementation of different measuring tools. A special acknowledgement is made to the GENCI CPU allocation concerning the French National Supercomputing centres TGCC and CINES, as well as the CALMIP Midi-Pyrénées supercomputing Centre. This work is carried out in the context of the HORIZON-2023-2027-PATHFINDER-Open-Project N° 101129952-BEALIVE-"Bioinspired Electroactive multiscale Aeronautical Live skin", http://smartwing.org/bealive/EU/ funded by the European Commission.

Copyright Statement

The authors confirm that they, and/or their company or organization, hold copyright on all of the original material included in this paper. The authors also confirm that they have obtained permission, from the copyright holder of any third party material included in this paper, to publish it as part of their paper. The authors confirm that they give permission, or have obtained permission from the copyright holder of this paper, for the publication and distribution of this paper as part of the ICAS proceedings or as individual off-prints from the proceedings.

7. References

1. Hoarau, Y., Pena, D., Vos, J., Charbonier, D., Gehri, A., Braza, M., Deloze T. and Laurendeau, E. (2016). Recent developments of the Navier-Stokes MultiBlock (NSMB) CFD solver. 54th AIAA Aerospace Sciences Meeting, San Diego, http://dx.doi.org/10.2514/6.2016-2056
2. Delbecq, S., Fontane, J., Gourdain, N., Mugnier, H., Planès, T. and Simatos, F. (2022). ISAE-SUPAERO - AVIATION AND CLIMATE: A LITERATURE REVIEW https://doi.org/10.34849/A66A-VV58
3. Scheller, J., "Electroactive morphing for the aerodynamic performance improvement of next generation airvehicles", PhD Thesis Institut National Polytechnique de Toulouse (INPT), https://www.theses.fr/189548525. Best thesis awards of INPT and GEET Doctoral School, as well as of DGA - Direction Générale de l'Armement at the 6th Innovation Forum of DGA, 7th December 2017.
4. Jodin, G., "Hybrid electroactive morphing at real scale - application to Airbus A320 wings", PhD thesis, Institut National Polytechnique de Toulouse, https://theses.fr/2017INPT0093, 25th October 2017. Best thesis awards of INPT and of the 3AF, October 2018.
5. Chinaud, M., Scheller, J., Rouchon, J-F., Duhayon, E., Braza, M. (2013) "Hybrid electroactive wings Morphing for aeronautic applications", *Solid State Phenomena* 198, pp. 200-205, 10.4028/www.scientific.net/SSP.198.200 .
6. Jodin, G., Motta, V., Scheller, J. Duhayon, E., Döll, C., Rouchon, J-F., Braza, M. (2017) "Dynamics of a hybrid morphing wing with active open loop vibrating trailing edge by time-resolved PIV and force measures", *Journal of Fluids and Structures*, 74, pp. 263-290, https://hal.archives-ouvertes.fr/hal-01638290.
7. Scheller, J., Jodin, G., Rizzo, K.J., Duhayon, E., Rouchon, J-F., Triantafyllou, M., Braza, M. "A Combined Smart-Materials Approach for Next-Generation Airfoils", *Solid-State Phenomena*, **251**, pp. 106-112, 2016, 10.4028/www.scientific.net/SSP.251.106.
8. Simiriotis, N., Jodin, G., Marouf, A., Elyakime, P., Hoarau, Y., Hunt, J., Rouchon, J.F. and Braza, M. (2019). "Morphing of a supercritical wing by means of trailing edge deformation and vibration at high Reynolds numbers: experimental and numercial investigation". *Journal of Fluids and Structures*, 91.https://doi.org/10.1016/j.jfluidstructs.2019.06.016
9. Dimino, I., Ciminello, M., Concilio, A., Pecora, R., Amoroso, F., Magnifico, M., Scheller, M., Gratias, A., Volovick, A. and Zivan, L. "Distributed actuation and control of a morphing wing trailing edge". In *Smart Intelligent Aircraft Structures (SARISTU)*, Springer, Cham, pp. 171–186, 2016. https://doi.org/10.1007/978-3-319-22413-8_9
10. Pecora, R., Amoroso, F. and Magnifico, M. "Towards the bi-modal camber morphing of large aircraft wing flaps: the CleanSky experience". Vol. 9801, pp. 98–106, 2016. https://doi.org/10.1117/12.2218415
11. Braza, M., Rouchon, J.-F., Tzabiras, G., Auteri, F. and Flaszynski, P. (2023). *Smart Morphing and Sensing for aeronautical configurations*; Prototypes, experimental and numerical findings from the H2020 N°723402 SMS EU Project; Notes on *Numerical Fluid Mechanics and Multidisciplinary Design* (Vol. 153). Springer, https://doi.org/10.1007/978-3-031-22580-2
12. Marouf, A., Hoarau, Y., Rouchon, J. and Braza, M**.** (2023). Three-dimensional simulation effects of trailing-edge actuation on a morphing A320 wing by means of hybrid turbulence modelling. *International Journal of Numerical Methods for Heat & Fluid Flow*, 33(4). https://doi.org/10.1108/HFF-09-2022-0559
13. Tô, J., Simiriotis, N., Marouf, A., Szubert, D., Asproulias, I., Zilli, D.M., Hoarau, Y., Hunt, J.C.R. and Braza, M. (2019). Effects of vibrating and deformed trailing edge of a morphing supercritical airfoil in transonic regime by numerical simulation at high Reynolds number.
Journal of Fluids & Structures,91. https://doi.org/10.1016/j.jfluidstructs.2019.02.011.
14. Jimenez-Navarro, C., Tô, J., Rouaix, C., Doerffer, P., Marouf, A., El Akoury, R. and Braza, M. (2024). Morphing effects on the aerodynamic performances of a supercritical wing's prototype in transonic flow conditions. In Advanced computational Methods and Design for Greener Aviation. *Computational Methods in Applied Sciences*, Springer. https://doi.org/10.1007/978-3-031-61109-4_11 .
15. Rouaix, C., Jimenez-Navarro, C., Carvalho, M., Raibaudo, C., Abou-Khalil, J., Marouf, A., Hoarau, Y., Harran, G., Hunt, J.C.R., Hangan, H., Rouchon, J.F. and Braza, M. (2023). Electroactive morphing effects on the aerodynamic performance through wobulation around an A320 wing with vibrating trailing edge at high Reynolds number. *Journal of Fluids and Structures*, 123. https://doi.org/10.1016/j.jfluidstructs.2023.104016.
16. Marouf, A., Charbonnier, D., Vos, J. B., El Akoury, R., Hoarau, Y., Braza, M. (2024). Morphing of high-lift wing-flap system with cambering and trailing-edge flapping at high Reynolds number towards a full airplane application. *Journal of Fluids and Structures*, 127, 104111, https://doi.org/10.1016/j.jfluidstructs.2024.104111
17. Simiriotis, N. "Numerical study and physical analysis of electroactive morphing wings and hydrodynamic profiles at high Reynolds number turbulent flows". PhD thesis, Institut National Polytechnique de Toulouse, 2020. http://www.theses.fr/2020INPT0041/document
18. Chorin, A.J., 1967. "A numerical method for solving incompressible viscous flow problems". *J. Comput. Phys.* 2 (1), 12–26. https://doi.org/10.1016/0021-9991(67)90037-X
19. Venkateswaran, S., Merkle, C., 1995. "Dual time-stepping and preconditioning for unsteady computations". In: 33rd Aerospace Sciences Meeting and Exhibit. American Institute of Aeronautics and Astronautics, https://doi.org/10.2514/6.1995-78
20. Jameson, A. « Energy Estimates for Nonlinear Conservation Laws with Applications to Solutions of the Burgers Equation and One-Dimensional Viscous Flow in a Shock Tube by Central Difference Schemes ». *18th AIAA Computational Fluid Dynamics Conference*, Miami, 2007. https://doi.org/10.2514/6.2007-4620

21. Szubert, D., Grossi, F., Jimenez-Garcia, A., Hoarau, Y., Hunt, J.C.R. and Braza, M. (2015). Shock-vortex shear-layer interaction in the transonic flow around a supercritical airfoil at high Reynolds number in buffet conditions. *Journal of Fluids and Structures,* Vol. 55, pp. 276-302, https://doi.org/10.1016/j.jfluidstructs.2015.03.005
22. Bourguet, R., Braza, M., Harran, G. and El Akoury, R. (2008). Anisotropic Organised Eddy Simulation for the prediction of non-equilibrium turbulent flows around bodies. *Journal of Fluids and Structures,* 24, 1240-1251. https://doi.org/10.1016/j.jfluidstructs.2008.07.004.
23. Braza, M., Perrin, R. and Hoarau, Y. (2006). Turbulence properties in the cylinder wake at high Reynolds numbers. *Journal of Fluids and Structures,* 22(6), 757-771. https://doi.org/10.1016/j.jfluidstructs.2006.04.021
24. Donea, J., Giuliani, S. and Halleux, J. (1982). An arbitrary lagrangian-eulerian finite element method for transient dynamic fluid-structure interactions. *Computer Methods in Applied Mechanics and Engineering*, 33(1-3), 689-723 https://doi.org/10.1016/0045-7825(82)90128-1
25. Abou Khalil, J., Maynard, N., Delon, X., El Akoury, R., Harran, G., Cazin, S., Marchal, M., Bergame, F., Ayroles, H., Rouchon, J-F. Braza, M. 15th EASN - International Conference on Innovation in Aviation & Space towards sustainability today and tomorrow | 14-17 October, 164 2025 | Madrid, Spain, Experimental Investigation of Electroactive Morphing on an A320 Prototype under Subsonic Take-Off Conditions.